Impact of g -factors and valleys on spin qubits in a silicon double quantum dot

Hwang, J.C.C.; Yang, C.H.; Veldhorst, M.; Hendrickx, N.; Fogarty, M. A.; Huang, W.; Hudson, F. E.; Morello, A.; Dzurak, A. S.

DOI
10.1103/PhysRevB.96.045302

Publication date
2017

Document Version
Final published version

Published in
Physical Review B (Condensed Matter and Materials Physics)

PHYSICAL REVIEW B **96**, 045302 (2017)

Impact of g-factors and valleys on spin qubits in a silicon double quantum dot

J. C. C. Hwang,[1,*] C. H. Yang,[1] M. Veldhorst,[1,2] N. Hendrickx,[3] M. A. Fogarty,[1] W. Huang,[1] F. E. Hudson,[1] A. Morello,[1] and A. S. Dzurak[1,†]

[1]*Centre for Quantum Computation and Communication Technology, School of Electrical Engineering and Telecommunications, The University of New South Wales, Sydney NSW 2052, Australia*

[2]*QuTech, TU Delft, 2600 GA Delft, The Netherlands*

[3]*University of Twente, P.O. Box 217, 7500 AE Enschede, The Netherlands*

(Received 27 February 2017; published 5 July 2017)

We define single electron spin qubits in a silicon metal-oxide-semiconductor double quantum dot system. By mapping the qubit resonance frequency as a function of a gate-induced electric field, the spectrum reveals an anticrossing that is consistent with an intervalley spin-orbit coupling. We fit the data from which we extract an intervalley coupling strength of 43 MHz. In addition, we observe a narrow resonance near the primary qubit resonance when we operate the device in the (1,1) charge configuration. The experimental data are consistent with a simulation involving two weakly exchanged-coupled spins with a Zeeman energy difference of 1 MHz, of the same order as the Rabi frequency. We conclude that the narrow resonance is the result of driven transitions between the T_- and T_+ triplet states, using an electron spin resonance signal of frequency located halfway between the resonance frequencies of the two individual spins. The findings presented here offer an alternative method of implementing two-qubit gates, of relevance to the operation of larger-scale spin qubit systems.

DOI: 10.1103/PhysRevB.96.045302

I. INTRODUCTION

The seminal proposal by Loss and DiVincenzo [1] for spin-based quantum computing using semiconductor quantum dots has led to numerous experimental demonstrations [2–6] and helped inspire the growing field of quantum spintronics [7]. Progress in silicon quantum dot qubits [8–10] has established promising coherence times, with as long as 28 ms [11] being achieved in isotopically purified ^{28}Si substrates [12]. The use of silicon as a device platform also has the advantage of sharing many similarities with standard manufacturing technologies used in today's microelectronics industry. Recently, universal quantum logic [13] in silicon has been demonstrated via the realization of single-qubit [11] and two-qubit logic gates [14], opening the path towards multiqubit coherent operations in silicon.

Previous work [14] illustrates that individual silicon quantum dots can possess local variability in the g-factor. By exploiting a gate-induced Stark shift, the g-factors of neighboring qubits can be tuned far apart with respect to their exchange interaction to enable high-fidelity controlled-Z (CZ) operations. In this paper, we analyze single electron spin qubits defined in a silicon metal-oxide-semiconductor (Si MOS) double quantum dot system and show that additional two-qubit gate operations can occur when the g-factors of neighboring qubits are close. In particular, our experimental data indicate that an electron spin resonance (ESR) frequency that is not in direct resonance with any of the individual qubits can simultaneously excite a pair of neighboring qubits. This effect has important implications for the scalability of silicon quantum dot systems, since while small g-factor differences may not provide the best setting for CZ operations [14], one could find it desirable and more flexible to operate two-qubit gates using a single ESR signal.

*jason.hwang@unsw.edu.au

†a.dzurak@unsw.edu.au

II. DEVICE CHARACTERIZATION

The quantum dot device, as shown in Fig. 1(b), consists of aluminum gates fabricated on an isotopically purified silicon epilayer substrate via multilayer gate stack technology [11,15]. A single electron transistor (SET) for charge sensing is fabricated next to four control gates (G1–G4), each of which can be independently tuned to locally define a quantum dot, as the aluminum oxide between neighboring gates forms natural tunnel barriers. Electrons are supplied to the quantum dots via a reservoir that is induced by a gate next to G4 that branches out from the SET top gate, so that the reservoir is connected to the SET drain. An on-chip broadband microwave line [16] for generating a high-frequency oscillating magnetic field is fabricated parallel to the device.

Using electrostatic confinement, we create a double quantum dot system under G1 and G2. This is tunnel coupled to an electron reservoir which extends under G3 and G4, since both these gates are biased well above threshold. The electron occupancy of each dot is electrically controlled via voltages applied to the gates. Figure 1(c) shows a charge stability diagram of the system, measured by the nearby SET charge sensor [17]. The charge occupancies of the relevant regions are labeled as (N1,N2), where N1 and N2 are the electron occupancies of dot 1 and dot 2, respectively. We can deplete both dots, under G1 and G2, respectively, to their last electron. The charge transitions as a function of the voltages on gates G1 and G2 form a characteristic honeycomb pattern, which demonstrates the electrostatic coupling between the dots.

Here, the spin states of a single electron under a static external magnetic field $B_0 = 1.45$ T are separated by the Zeeman splitting, $E_Z = g\mu_B B_0$, where g is the electron g-factor and μ_B is the Bohr magneton. By applying a high-frequency oscillating current through the on-chip microwave antenna, an oscillating magnetic field is generated. Coherent control of the qubit is achieved when the frequency of this ac magnetic field matches the electron Zeeman splitting.

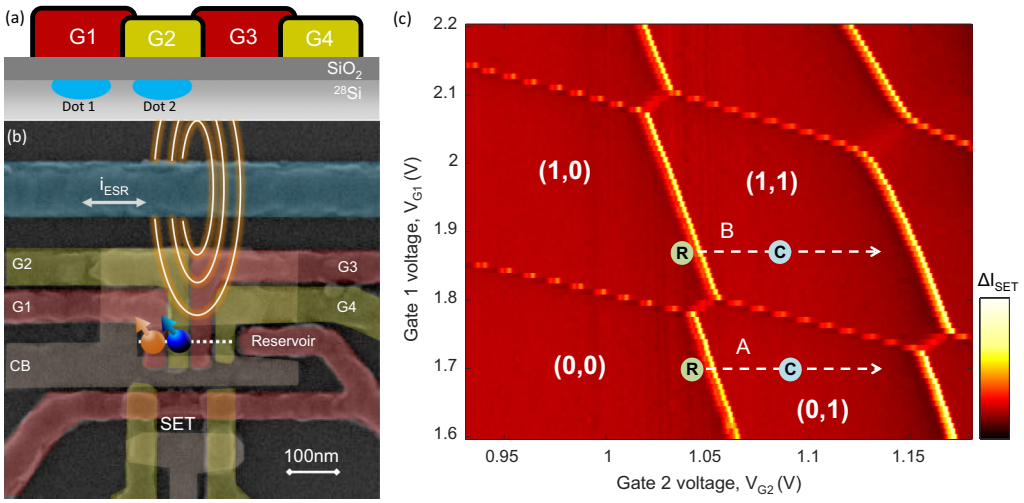

FIG. 1. (a) Cross-sectional schematic along the white dotted line in (b), and (b) scanning electron microscope image of the Si MOS quantum dot device. Multilayer aluminum gate electrodes are patterned using electron beam lithography. The aluminum oxide that serves as an insulator between gates also forms a natural tunnel barrier between the double dots that are formed under G1 and G2. An adjacent SET is used to monitor the charge occupancy of the dot while a microwave antenna allows coherent control of the qubit via ESR. (c) Charge stability diagram of a coupled double dot system, as a function of gate voltages V_{G1} and V_{G2}.

Single-shot measurement of the qubit state is performed via an electron spin-to-charge conversion [18].

Two-qubit gates [14] can be realized by initializing the qubits in the (1,1) charge state and switching on the exchange interaction via fast gate pulsing towards the (0,2) transition. In the current experiment, however, we only have high-frequency pulse control of G2 and not G1. As a result, we cannot pulse diagonally towards the (1,1)−(0,2) transition. The high tunnel rate between dot 1 (under G1) and the reservoir also prohibits us from reading the spin state of this dot. Therefore, in this work, we rely on pulsing and reading dot 2 only, to characterize the device in the (1,1) charge region.

III. SPIN-VALLEY MIXING

A standard two-level pulse sequence [see Fig. 2(a)] is applied to gate G2 in order to map out the resonance frequency of the electron spin qubit formed in dot 2 as a function of plunge level V_{G2}. Stark shifting of the electron g-factor via the electric field has been experimentally reported in a similar device [11,19], where the plunger gate voltage has direct control over the out-of-plane electric field through the quantum dot, and hence the qubit resonance frequency. In this device, an expected linear dependency of qubit resonance frequency on the plunge level is observed (Appendix A) when the qubit is operating in the (0,1) charge region, as marked by A in Fig. 1(c). Here, (C) and (R) represent the qubit control and readout/initialization position, respectively. The gate-pulsing sequence applied at (C) and (R) are shown in Fig. 2(a).

When the qubit system is operated in the (1,1) charge region, labeled B in Fig. 1(c), we obtain an ESR spectrum [Fig. 2(b)] that contains multiple resonance branches. Coherent Rabi oscillations can be obtained at the two bright branches. Anticrossings in the frequency spectrum are also revealed, which are the result of coupling to another degree of freedom. To investigate the origin of these anticrossings, the ESR spectrum was mapped out at several different values of V_{G1} and at two different magnetic fields, and the corresponding location of the anticrossing point was measured in terms of the plunge level V_{G2} where ESR was performed (Appendix B).

Due to the gate voltage dependence of the anticrossing, the additional state is likely to be another charge state, or an excited valley state, and we consider the likelihood of each possibility in turn. We first consider the possibility of a charge transition. It is immediately clear that the locus of the anticrossing occupies the center of the (1,1) charge region (Appendix B), indicating that a charge state is unlikely to be the cause, as this would require the ESR plunge level to be very close to the (1,1)−(0,2) or (1,1)−(1,2) charge transition. This is further rejected by the observation of the resonances bending upward to the left of the anticrossing and downward to the right, which indicates the energy of the state increases with increasing V_{G2} gate voltage, a trend that is directly opposite to what a (0,2) or (1,2) charge state would exhibit when $|\downarrow,\downarrow\rangle$ is the ground state of the system [14].

Next, we consider the possibility of an excited valley state, and note that a similar type of anticrossing has been observed previously [20] and can be attributed to intervalley spin-orbit coupling [20], which occurs when the valley splitting equals the Zeeman splitting, $E_{VS} = E_Z$. The sixfold valley degeneracy in the conduction band of bulk silicon is lifted via confinement of electrons in a quantum dot, leaving two low-lying valley states with energy scales relevant to the spin qubit operation. It has been experimentally demonstrated that the valley splitting E_{VS} in a quantum dot is dependent on the out-of-plane electric field [21] and can be controlled using gate potential over a range of 0.5 meV [11,21].

Figure 2(c) shows the energy level diagram of a model based on valley states we devised for generating the fittings (blue and green dotted lines) overlaid on the experimental data in Fig. 2(b). The fit Hamiltonian is included in Appendix C.

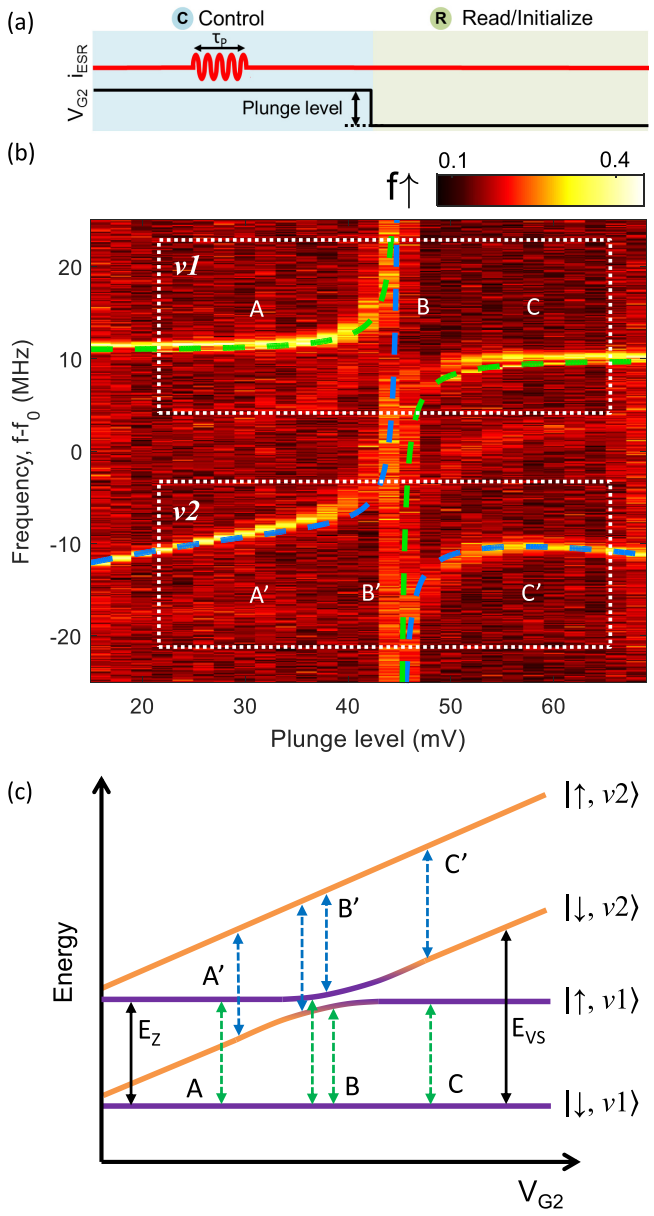

FIG. 2. (a) Gate-pulse sequence for ESR control. An ESR microwave burst of pulse length τ_p is applied to the qubit, followed by spin readout and initialization of a spin-down electron for the next control pulse. (b) ESR spectrum, showing the electron spin-up fraction $f\uparrow$ as a function of qubit resonance frequency and G2 plunge level. The external magnetic field is set at 1.45 T, with voltage operating points $V_{G1} = 1.87$ V and $V_{G2} = 1.047$ V. The resonance frequency $f_0 = 40.23$ GHz and $\tau_p = 50$ μs. The resonances are fitted by dashed lines, with a color code described by (c), which is a model of a quantum dot incorporating both spin and valley degrees of freedom.

The model assumes a single quantum dot with E_{VS} tunable via the voltage on G2. Mixing between $|\uparrow, v1\rangle$ and $|\downarrow, v2\rangle$ states occurs when the valley splitting energy approximately equals the Zeeman energy, and modifies the resonance frequency of the qubit. From the model we extract an intervalley coupling strength $\beta = 43$ MHz. We find experimentally that a 40 mV change on V_{G2} is required to offset the anticrossing energy by an equivalent amount to a change in magnetic field of 0.1 T (Appendix B). In a similar Si MOS quantum dot device [21] the same level of energy tuning required a 18 mV change on the plunger gate potential. The energy tuning for both devices is of a similar order of magnitude, and the small difference is most likely attributed to differences in the voltage biasing arrangement between the two devices.

An ESR-driven spin transition within a valley should produce only a single resonance in the spectrum; our observation of two resonances could be explained if we assume that the qubit can be initialized to the spin-down state of either valley [10], and that the two valleys have a g-factor difference of approximately 20 MHz. During spin readout/initialization, E_{VS} is smaller than E_Z, and so the Fermi level of the reservoir can be positioned between the spin-down and spin-up states of the two valleys [left side of Fig. 2(c)]. E_{VS} is then subsequently increased due to the deeper plunge level during ESR control, where the spin qubit is driven in either one of the two valleys. With the aforementioned tunability of $E_{VS}/g\mu_B$ corresponding to 0.1 T per 40 mV on the plunger gate, this implies that at the readout position, the gap for differentiating between $|\downarrow, v2\rangle$ and $|\uparrow, v1\rangle$ is around $g\mu_B(0.11\text{ T}) \approx 13$ μeV. The valley initialization assumption further indicates the valley

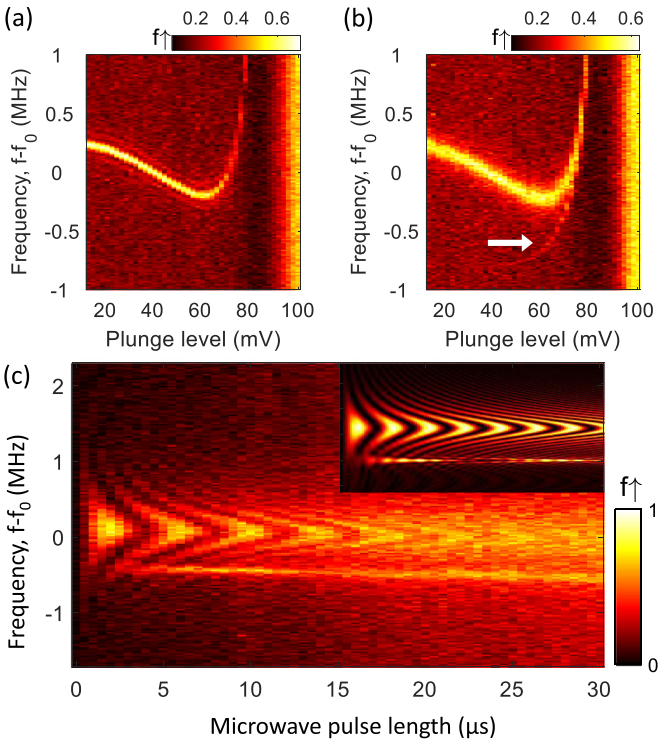

FIG. 3. (a) Electron spin-up fraction $f\uparrow$ as a function of qubit resonance frequency and ESR plunge level, with $V_{G1} = 1.87$ V and $f_0 = 42.947$ GHz. The ESR microwave pulse length is applied for 14 μs. Clear nonlinearity in the resonance branch can be seen. (b) An additional level appears beneath the main branch when the same measurement is repeated with a longer microwave pulse length of 214 μs. (c) Rabi oscillation obtained at $V_{G1} = 1.82$ V, with $f_0 = 42.972$ GHz. Adjacent to the main Rabi chevron pattern is a narrow oscillation branch, which is associated with the faint resonance observed in (b). Inset: The corresponding simulated Rabi oscillation by measuring only dot 2, with a Zeeman energy difference between the two dots $\delta E_Z = 1$ MHz and Heisenberg exchange coupling $J = 250$ kHz.

relaxation time in our system is long, at least longer than the dot 2 plunge time of 950 μs. This falls within the range of possible valley relaxation times predicted recently in Ref. [22], where the valley relaxation rate is estimated to be a strong function of the relative location of the quantum dot to a step at the Si-SiO_2 interface.

IV. ESR DRIVEN TWO-SPIN ROTATIONS

We now focus our attention on the small frequency splitting that is seen in the upper resonance branch before and after the anticrossing. We perform higher-resolution mapping of the ESR spectrum in that region, as shown in Fig. 3(a), with the magnetic field set at 1.55 T and the microwave pulse length at 14 μs. The anticrossing seen in Fig. 2(b) is shifted in location as the gate voltages of G1 and G2 are changed. The dramatic increase in the spin-up fraction at the far right of the map is simply the result of changes in the SET current level due to loading of another electron as we approach the (1,1)−(1,2) charge transition using a deeper plunge level.

Repeating the same measurement with a longer microwave pulse length reveals an additional resonance which appears near the bending of the resonance branch, as shown in Fig. 3(b). This divergent resonance corresponds to the narrow resonance next to the primary Rabi chevron pattern [11] in Fig. 3(c), where we plot the electron spin-up fraction as a function of microwave pulse length and frequency detuning.

As we do not observe this extra resonance frequency when the qubit is operated in the (0,1) charge region, this leads us to the belief that we observe an effect related to coupling with the adjacent qubit in dot 1. Indeed, we can closely match the experimental data with a simulated Rabi oscillation [inset of Fig. 3(c)] in which we assume that the spin in dot 2 is weakly exchange coupled to that in dot 1 ($J = 250$ kHz) where the two dots have a different Zeeman energy $\delta E_Z = \delta g \mu_B B_0 = 1$ MHz due to their difference in g-factor, δg. The system Hamiltonian in the rotating-wave approximation is given in Eq. (1), with the basis $\{|\uparrow,\uparrow\rangle, |\uparrow,\downarrow\rangle, |\downarrow,\uparrow\rangle, |\downarrow,\downarrow\rangle\}$,

$$\begin{pmatrix} -\Delta\omega - \frac{1}{2}\delta E_Z & \Omega & \Omega & 0 \\ \Omega & \frac{1}{2}\delta E_Z - \frac{1}{2}J & \frac{1}{2}J & \Omega \\ \Omega & \frac{1}{2}J & -\frac{1}{2}\delta E_Z - \frac{1}{2}J & \Omega \\ 0 & \Omega & \Omega & \Delta\omega + \frac{1}{2}\delta E_Z \end{pmatrix}, \tag{1}$$

where $\Delta\omega$ is the microwave frequency minus the Larmor frequency of spin 2, and Ω is the Rabi frequency. $J = \frac{2t^2}{U-\epsilon-\delta E_Z} + \frac{2t^2}{U-\epsilon+\delta E_Z}$, as derived in the Supplemental Material of Ref [14], is an effective exchange arising from tunnel coupling between the $|\uparrow,\downarrow\rangle, |\downarrow,\uparrow\rangle$ state and the (0,2) state, where U is the on-site Coulomb energy and ϵ the detuning. The simulation only measures the z component of spin 2, which corresponds to reading out only dot 2 in the experiment. Further details on the Rabi simulation are included in Appendixes D and E.

When the applied microwave frequency is halfway between the two qubits' resonance frequencies, and given that there is a finite exchange coupling, the two qubits are excited simultaneously from T_- ($|\downarrow,\downarrow\rangle$) to T_+ ($|\uparrow,\uparrow\rangle$). Since we only perform readout on dot 2, the ESR chevron pattern of the other spin is absent from Fig. 3(c), and the narrow-band resonance corresponds to the flipping of T_- to T_+. This operation originates from a second-order effect via the $|\uparrow,\downarrow\rangle$ and $|\downarrow,\uparrow\rangle$ states which creates an effective coupling C_{eff} between the two triplet states. The resulting Hamiltonian approximated from second-order perturbation on Eq. (1) is given as follows ($\delta E_Z > J$ for the approximation to hold),

$$\begin{pmatrix} -\Delta\omega - \frac{1}{2}\delta E_Z & C_{\text{eff}} \\ C_{\text{eff}} & \Delta\omega + \frac{1}{2}\delta E_Z \end{pmatrix} \begin{pmatrix} |\uparrow,\uparrow\rangle \\ |\downarrow,\downarrow\rangle \end{pmatrix}, \tag{2}$$

where $C_{\text{eff}} = 4J\Omega^2/(\delta E_Z^2 - J^2)$ (see Appendix E for the derivation). This indicates the coupling diminishes to zero for large δE_Z and only becomes visible when δE_Z reduces to a similar order of magnitude as the exchange.

The two-spin rotation here is a combination of imaginary SWAP (iSWAP) and $X(\pi)$ rotation on both qubits, with their Hamiltonians defined in Fig. 4(a). By applying half the duration of the microwave pulse, a universal two-qubit gate can be realized. For example, a controlled-NOT (CNOT) can be constructed as shown in Fig. 4(b).

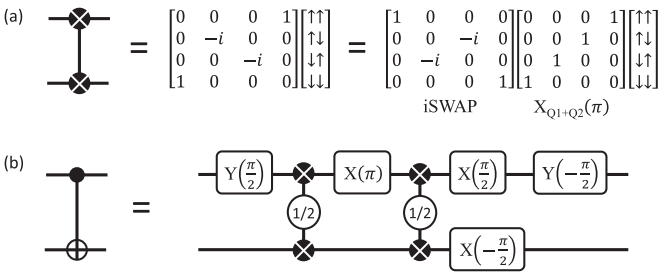

FIG. 4. (a) The two-spin rotation is a combination of iSWAP and $X(\pi)$ on both qubits. (b) The decomposition of a CNOT gate into two-spin rotations and single-qubit gates. The 1/2 denotes the application of the two-qubit gate in (a) with half the duration.

V. CONCLUSION

In conclusion, we have analyzed a spin qubit formed in a Si MOS double quantum dot system, where the qubit is weakly exchange coupled to a neighboring spin. The ESR spectrum shows an anticrossing in the resonance frequency that is consistent with an intervalley spin-orbit coupling, with a strength of 43 MHz. Previous qubit devices [14] reported a δE_Z between two neighboring dots that varies between 20 and 40 MHz. The findings here also reveal a mechanism that can be exploited for qubit operations when the g-factor difference is

small, with our simulation result suggesting a δE_Z of 1 MHz. This has allowed us to observe ESR-driven transitions between the T_- and T_+ state, which requires only the use of a single ESR pulse to simultaneously rotate two individual spins. This could be used in future to add flexibility to qubit operations in large-scale silicon quantum dot systems.

ACKNOWLEDGMENTS

The authors thank D. Culcer for enlightening discussions. We thank D. Barber and R. Ormeno for technical support in the measurement laboratory. This work was supported by the Australian Research Council (CE11E0001017), the U.S. Army Research Office (W911NF-13-1-0024), and the NSW Node of Australian National Fabrication Facility.

APPENDIX A: LINEAR STARK SHIFT OF QUBIT RESONANCE FREQUENCY

When the qubit is operated in the (0,1) charge region, as marked by trajectory (A) in Fig. 1(b), the resonance frequency as a function of both the plunger gate and the barrier gate voltages are found to be linear, with their relative contribution to the electric field $\frac{dF/dV_{G1}}{dF/dV_{G2}} = R_{F,V_{G1}V_{G2}} = -2.68$ (see Fig. 5). We have performed simulations using the Synopsys Sentaurus Semiconductor TCAD Software and found a ratio $R_{F,V_{G1}V_{G2}} = -2.62$, which shows excellent agreement with the experimental value.

APPENDIX B: ANTICROSSING LOCATION

The location of the anticrossing in Fig. 2 in the main text is highly dependent on gate voltages. We perform similar ESR spectrum mapping at several different gate voltages of G1 and measure the voltage G2 required to plunge from the spin readout level to reach the anticrossing. The experiment is also performed under two different external magnetic field (1.55 and 1.45 T) and the resulting anticrossing position is plotted on the charge stability map in Fig. 6.

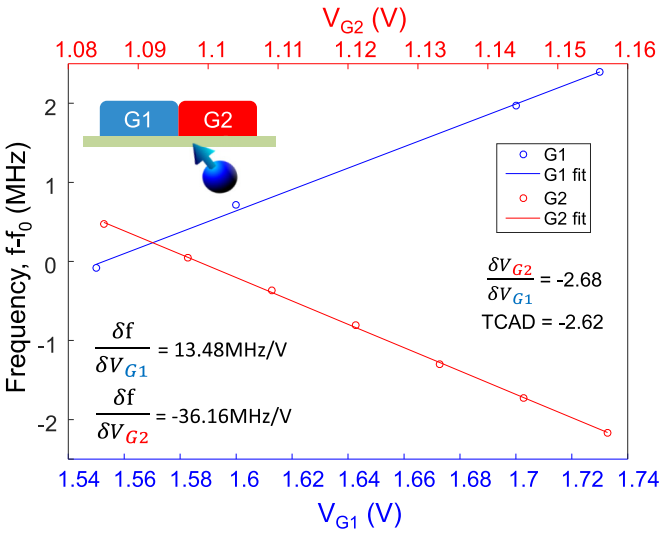

FIG. 5. Qubit resonance frequency as a function of barrier gate voltage G1 (blue) and plunger gate G2 (red).

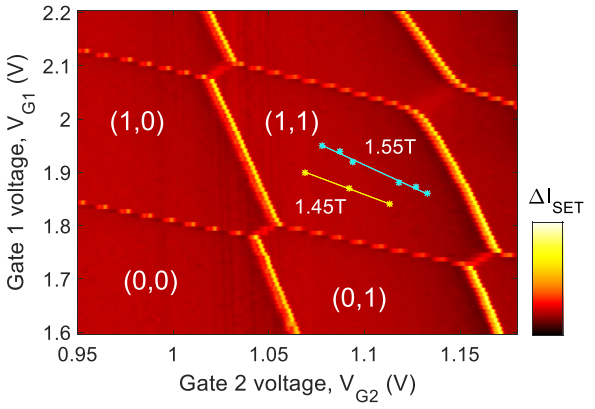

FIG. 6. Anticrossing location as a function of V_{G1}. The locus is plot out for two different magnetic field magnitudes.

APPENDIX C: FITTING OF THE ESR SPECTRUM

The fitting of Fig. 2 in the main text is achieved with a model that considers the spin states of a single electron, Zeeman splitted by a dc magnetic field, and takes into account of the valley degree of freedom. The static Hamiltonian is a simple 4×4 matrix, with the basis being $|\uparrow,v1\rangle, |\uparrow,v2\rangle, |\downarrow,v1\rangle, |\downarrow,v2\rangle$,

$$H = \begin{pmatrix} \frac{E_{Z,v1}+E_{Z,v2}}{2} + E_{VS} & 0 & 0 & 0 \\ 0 & \frac{E_{Z,v1}-E_{Z,v2}}{2} + E_{VS} & \beta & 0 \\ 0 & \beta & E_{Z,v2} & 0 \\ 0 & 0 & 0 & 0 \end{pmatrix}, \tag{C1}$$

where $E_{Z,v1}$ and $E_{Z,v2}$ are the Zeeman splittings in the upper and lower valley. The valley splitting E_{VS} is dependent on the electric field through the dot, which is in turn dependent on the gate voltage. In the model we assume a valley splitting tunability of 640 μeV/V as quoted in Ref. [21]. Valley states become relevant when either E_{VS} is very small or when E_{VS} is in the order of the Zeeman splitting, with the latter being the case for our fitting. β is the intervalley coupling parameter, which involves a spin flip.

APPENDIX D: RABI SIMULATION

The Hamiltonian in Eq. (1) that describes two spins with Heisenberg exchange coupling is used in the Rabi simulation. By assuming a fixed δE_Z of 1 MHz and setting $J = 0$ and 250 kHz, we obtain the two Rabi maps as shown in Fig. 7.

Furthermore, by fixing J at 250 kHz, and varying δE_Z, we can observe the evolution of a narrow resonance adjacent to the main Rabi, as shown in Fig. 8. As δE_Z decreases, the narrow resonance broadens and moves closer to the main Rabi, and then passes to the other side as δE_Z becomes negative.

APPENDIX E: EFFECTIVE COUPLING BETWEEN THE $|\uparrow,\uparrow\rangle$ AND $|\downarrow,\downarrow\rangle$ STATES

In this Appendix we look at the effective coupling between the $|\uparrow,\uparrow\rangle$ and $|\downarrow,\downarrow\rangle$ states. We begin with the Hamiltonian of

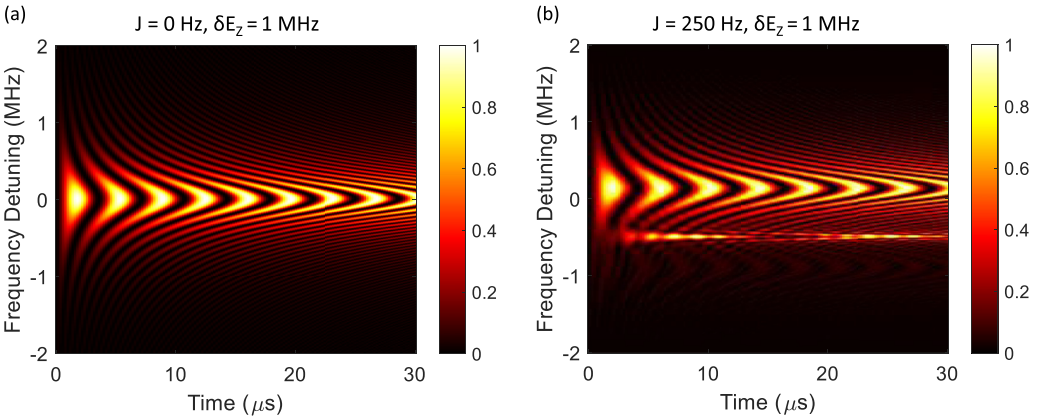

FIG. 7. Rabi simulation assuming $\delta E_Z = 1$ MHz and (a) $J = 0$ Hz, (b) $J = 250$ kHz.

Eq. (1) in the main text,

$$\begin{pmatrix} -\Delta\omega - \frac{1}{2}\delta E_Z & \Omega & \Omega & 0 \\ \Omega & \frac{1}{2}\delta E_Z - \frac{1}{2}J & \frac{1}{2}J & \Omega \\ \Omega & \frac{1}{2}J & -\frac{1}{2}\delta E_Z - \frac{1}{2}J & \Omega \\ 0 & \Omega & \Omega & \Delta\omega + \frac{1}{2}\delta E_Z \end{pmatrix}. \tag{E1}$$

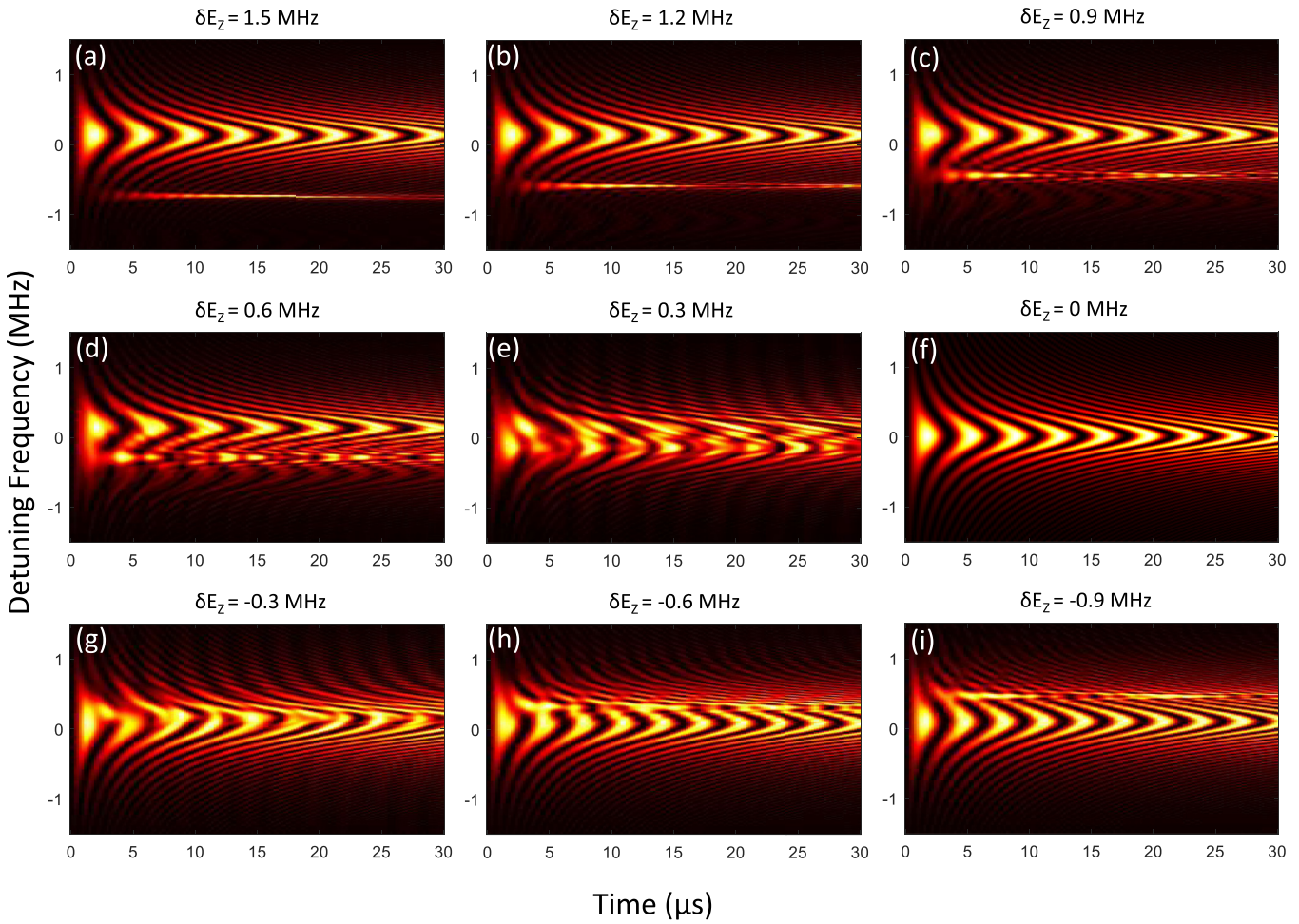

FIG. 8. Evolution of Rabi oscillation as a function of g-factor difference δE_Z, with J fixed at 250 MHz.

We can find an effective coupling C_{eff} between the $|\uparrow,\uparrow\rangle$ and $|\downarrow,\downarrow\rangle$ by applying a second-order perturbation approximation to Eq. (E2),

$$\begin{pmatrix} -\Delta\omega - \frac{1}{2}\delta E_Z & C_{\text{eff}} \\ C_{\text{eff}} & \Delta\omega + \frac{1}{2}\delta E_Z \end{pmatrix}, \tag{E2}$$

$$C_{\text{eff}} = \frac{4J\Omega^2\left[J^2 - 2\left(\delta E_Z^2 + 2\delta E_Z \Delta w + 2\Delta w^2\right)\right]}{(J - 2\Delta w)(2\Delta w + J)[J - 2(\delta E_Z + \Delta w)][2(\delta E_Z + \Delta w) + J]}. \tag{E3}$$

As the simultaneous rotation of the two spins occurs in the vicinity of halfway between the two qubits' resonance frequencies, Eq. (E3) can then be simplified by letting $\Delta\omega = -\frac{1}{2}\delta E_Z$,

$$C_{\text{eff}} \approx \frac{4J\Omega^2}{\delta E_Z^2 - J^2}. \tag{E4}$$

[1] D. Loss and D. P. DiVincenzo, Phys. Rev. A **57**, 120 (1998).
[2] J. R. Petta, A. C. Johnson, J. M. Taylor, E. A. Laird, A. Yacoby, M. D. Lukin, C. M. Marcus, M. P. Hanson, and C. Gossard, Science **309**, 2180 (2005).
[3] F. H. L. Koppens, C. Buizert, K. J. Tielrooij, I. T. Vink, K. C. Nowack, T. Meunier, L. P. Kouwenhoven, and L. M. K. Vandersypen, Nature (London) **442**, 766 (2006).
[4] K. C. Nowack, M. Shafiei, M. Laforest, G. E. D. K. Prawiroatmodjo, L. R. Schreiber, C. Reichl, W. Wegscheider, and L. M. K. Vandersypen, Science **333**, 1269 (2011).
[5] M. D. Shulman, O. E. Dial, S. P. Harvey, H. Bluhm, V. Umansky, and A. Yacoby, Science **336**, 202 (2012).
[6] J. Medford, J. Beil, J. M. Taylor, S. D. Bartlett, A. C. Doherty, E. I. Rashba, D. P. DiVincenzo, H. Lu, A. C. Gossard, and C. M. Marcus, Nat. Nanotechnol. **8**, 654 (2013).
[7] D. D. Awschalom, L. C. Bassett, A. S. Dzurak, E. L. Hu, and J. R. Petta, Science **339**, 1174 (2013).
[8] B. M. Maune *et al.*, Nature (London) **481**, 344 (2012).
[9] D. Kim *et al.*, Nature (London) **511**, 70 (2014).
[10] E. Kawakami, P. Scarlino, D. R. Ward, F. R. Braakman, D. E. Savage, M. G. Lagally, M. Friesen, S. N. Coppersmith, M. A. Eriksson, and L. M. Vandersypen, Nat. Nanotechnol. **9**, 666 (2014).
[11] M. Veldhorst *et al.*, Nat. Nanotechnol. **9**, 981 (2014).
[12] K. M. Itoh and H. Wanatabe, MRS Commun. **4**, 143 (2014).
[13] M. A. Nielsen and I. L. Chuang, *Quantum Computation and Quantum Information* (Cambridge University Press, Cambridge, U.K., 2000).
[14] M. Veldhorst *et al.*, Nature (London) **526**, 410 (2015).
[15] S. J. Angus, A. J. Ferguson, A. S. Dzurak, and R. G. Clark, Nano Lett. **7**, 2051 (2007).
[16] J. P. Dehollain, J. J. Pla, E. Siew. K. Y. Tan, A. S. Dzurak, and A. Morello, Nanotechnology **24**, 015202 (2012).
[17] C. H. Yang, W. H. Lim, F. A. Zwanenburg, and A. S. Dzurak, AIP Adv. **1**, 042111 (2011).
[18] J. M. Elzerman, R. Hanson, L. H. Willems van Beveren, B. Witkamp, L. M. K. Vandersypen, and L. P. Kouwenhoven, Nature (London) **430**, 431 (2004).
[19] M. Veldhorst, R. Ruskov, C. H. Yang, J. C. C. Hwang, F. E. Hudson, M. E. Flatté, C. Tahan, K. M. Itoh, A. Morello, and A. S. Dzurak, Phys. Rev. B **92**, 201401(R) (2015).
[20] X. Hao, R. Ruskov, M. Xiao, C. Tahan, and H. W. Jiang, Nat. Commun. **5**, 3860 (2014).
[21] C. H. Yang, A. Rossi, R. Ruskov, N. S. Lai, F. A. Mohiyaddin, S. Lee, C. Tahan, G. Klimeck, A. Morello, and A. S. Dzurak, Nat. Commun. **4**, 2069 (2013).
[22] P. Boross, G. Széchenyi, D. Culcer, and A. Pályi, Phys. Rev. B **94**, 035438 (2016).